Energy Technology
Generation, Conversion, Storage, Distribution
www.entechnol.de

Dielectric Barrier Discharge Reactors for Plasma-Assisted CO_2 and CH_4 Conversion: A Comprehensive Review of Reactor Design, Performance, and Future Prospects

*Md Robayet Ahasan, Md Monir Hossain, and Ruigang Wang**

Dielectric barrier discharge (DBD) plasma is a promising technology for catalysis due to its low-temperature operation, cost-effectiveness, and silent operation. This review comprehensively analyzes the design and operational parameters of DBD plasma reactors for three key catalytic applications: CH_4 conversion, CO_2 splitting, and dry reforming of methane (DRM). While catalyst selection is crucial for achieving desired product selectivity, reactor design and reaction parameters such as discharge power, electrode gap, reactor length, frequency, dielectric material thickness, and feed gas flow rate, significantly influence discharge characteristics and reaction mechanisms. This review also explores the influence of less prominent factors, such as electrode shape and applied voltage waveforms. Additionally, this review addresses the challenges of DBD plasma catalysis, including heat loss, temperature effects on discharge characteristics, and strategies for enhancing overall efficiency.

1. Introduction

Climate change on the earth is now causing huge concerns due to the increase in the global average temperature. The emission of greenhouse gases such as carbon dioxide (CO_2) and methane (CH_4) from burning fossil fuels is primarily responsible for this global temperature change.[1] On the contrary, the global energy demand is increasing due to population growth, expanding industrial activities, and ongoing economic growth. Although there is a high demand for fast-growing renewable energy, conventional fossil fuels still dominate in meeting this demand. Around 78% of world primary energy demand is provided by oil, natural gas, and coal,[2] where CO_2 produced from these fuels is responsible for 71.6% of greenhouse gas emissions in 2022.[3] Thus, a unique, sustainable, and long-lasting solution must address these challenges. The utilization of catalytic chemical reaction technology for the conversion of greenhouse gases such as CO_2 and CH_4 into fuels and valuable chemicals represents an appealing solution.[4] Over the past decades, based on the research and development of advanced materials, reactor design, reaction mechanism studies, and scale-up technologies (i.e., modular and intensified conversion), various strategies and methods have been utilized for CO_2/CH_4 capturing, storage, and conversion to produce valuable fuels/chemicals via thermochemical,[5] electrochemical,[6] and photochemical technology.[7] However, these lab-scale research and/or commercial technologies are still facing challenges for poor conversion efficiency, high-cost,[8] high equipment corrosion, and high energy consumption, which often require high temperature, pressure,[9] and complex systems. Therefore, it is imperative to explore new economically viable ways to harness these greenhouse gases into useful chemical products and fuels under low or mild temperatures and pressure.[10–14]

Recently, nonthermal and/or nonequilibrium processes, such as nonequilibrium plasma-assisted CO_2/CH_4 catalytic conversion, have emerged as promising alternatives to address the limitations of the previously mentioned thermal/electrochemical/photoelectrical conversion technology as well as promoting the conversion efficiency and product selectivity. Plasma catalysis has garnered significant scholarly attention due to its high impact of ionization avalanches on converting CO_2 and CH_4 gases and NH_3 synthesis at a cost-effective process. Additionally, the plasma-assisted system features straightforward reactor designs, rapid reaction rates, enhanced activity, and efficient reactor and thermal management (i.e., the ability to switch plasma on and off instantly).[15–18] The rationale behind plasma-assisted thermal catalysis is that it combines plasma-induced excited species, ions, and radicals with conventional catalytic materials. It can drive non-thermodynamically equilibrium reactions into desired products at moderate temperature and pressure. For example, in the plasma-assisted catalytic reaction, electrons, ions, and radicals are generated at the catalyst region of the reactor so that plasma and catalyst interact, and this interaction enhances the reaction performance. Consequently, the synergism of plasma and catalyst promotes different reactions, including ammonia synthesis[19–21] and CH_4 and CO_2 reforming reactions[22–26] with particular products at low temperatures.

M. R. Ahasan
Department of Metallurgical and Materials Engineering
The University of Alabama
Tuscaloosa, AL 35487, USA

M. M. Hossain, R. Wang
Department of Chemical Engineering and Materials Science
Michigan State University
East Lansing, MI 48824, USA
E-mail: rwang@msu.edu

The ORCID identification number(s) for the author(s) of this article can be found under https://doi.org/10.1002/ente.202401177.

DOI: 10.1002/ente.202401177

Many plasma generation technologies and reactors have been developed because of the proper utilization of the synergistic effect of plasma catalysis. For example, dielectric barrier discharge (DBD) reactor,[27–29] microwave (MW) plasma reactor,[30–32] corona discharge (CD) reactor,[33–35] and gliding arc plasma (GAP) reactor[36–39] have been utilized to perform plasma-assisted catalytic reactions. To optimize the generation of plasma discharge and plasma-catalysis synergy, researchers have proposed or executed several modifications of these reactors in different experiments to improve the performance parameters in plasma-assisted catalytic reactions.

Although many experimental efforts have been reported to improve the conversion rate and efficiency of plasma-assisted catalytic gas conversion, data remain limited of these heterogeneous chemistry/processes and the correlation of performance parameters with reactor geometry. The fundamental understanding of plasma-assisted catalytic gas conversion is still limited. Several approaches and reactor designs have been conducted to improve selectivity, conversion rate, and efficiency, but a stable, optimal solution is still being sought. More research on the plasma-assisted catalytic reactor design is needed to reveal clear and detailed information on how reactor geometry, catalyst, and plasma–catalyst interaction influence conversion rate and efficiency. In addition, analysis techniques for plasma-catalysis experiment monitoring should also be obtained in situ to better understand the intermediate species, active sites, and plasma–catalyst interaction.[40–42] Thus, further research is required to understand the underlying causes of the plasma-assisted catalytic mechanism to improve its performance parameters, such as product selectivity, conversion rate, and efficiency.

This review aims to provide a detailed overview of the available information on DBD plasma-assisted catalytic reactors for converting greenhouse gas (CH_4, CO_2). Here, we primarily focus on individual or simultaneous CH_4 and CO_2 conversion methods because two reactants negatively impact gas compounds. Moreover, one of the purposes of this review is to identify the essential factors of reactor geometry influencing plasma-assisted catalytic reaction.

2. Possible Routes of CO_2 and CH_4 Conversion

Thermal catalysis has been a longstanding way to convert CO_2 and CH_4 into valuable chemical products. **Table 1** lists some common chemical reactions with corresponding enthalpy and Gibb's energy for converting CO_2 and CH_4, where these gases act as feedstock to produce C_2H_6, R—CHO, R—OH, CO, H_2, and H_2O.

Among the reactions mentioned above, dry reforming of methane (DRM, Equation (6)) is one of the most appealing processes for converting two major greenhouse gases: CH_4 and CO_2. One of the significant challenges for the practical DRM application lies in its high operating temperature above 850 °C[43] under relatively high pressure of ≈1–20 atm[44,45], which is due to the high binding energy of C═O (532 kJ mol^{-1}) and C—H (434 kJ mol^{-1}) in CO_2 and CH_4, respectively.[46] Therefore, the high bond activation energy requirements for CO_2 and CH_4 dissociation make direct or indirect thermal conversion methods underprivileged in conversion rate and efficiency. Overall, thermal catalysis of DRM is not energy-efficient at low temperatures (<500 °C), and the conversions and yields are typically very low (<20%) at lower temperatures.[47,48] In addition, conventional thermal conversion requires a high-quality reactor configuration to overcome the thermodynamic barrier, which makes the conventional reactions economically unfavorable.[49]

3. Thermal Versus Plasma-Assisted Catalytic DRM Process

Figure 1a,b shows schematics of pure thermal and plasma-assisted catalytic reaction mechanisms for DRM reaction ($CH_4 + CO_2 \rightarrow 2CO + 2H_2$) in a comparable way. As shown in Figure 1a, for thermal conversion of CH_4, molecular collision and C—H activation kinematics occur under "extreme environments" such as high temperatures (i.e., in the range of 850–1000 °C) due to the relatively high dissociation energy of its C—H bond (434 kJ mol^{-1}). The high-temperature thermal catalytic DRM conversion also faces issues, including catalyst sintering, coking, and low product selectivity.[50]

For plasma-assisted catalytic conversion of DRM shown in Figure 1b, various radicals, ions, electrons, and excited intermediate species are generated through plasma-assisted catalytic reaction pathways, mainly driven by high-energy electrons and ionized species.[51] These excited species, normally unavailable under a thermal reaction process, present a great advantage of a plasma-assisted catalytic reactor that can operate under relatively mild conditions. Thus, highly energetic electrons and abundant radicals/ions in a plasma-assisted catalytic reactor can replace high temperature and pressurized conditions typically required in a thermal catalytic reactor.

In DRM application, thermal catalysis is inefficient at low temperatures (<500 °C), whereas plasma catalysis shows excellent

Table 1. Enthalpy and Gibb's energy for selected conversion reactions of CO_2 and CH_4.

Chemical reaction		ΔH_r [kJ mol^{-1}]	ΔG_r [kJ mol^{-1}]	References
$CO_2(g) + H_2(g) \rightarrow HCOOH(l)$	(1)	−31.0	+34.3	[125]
$CO_2(g) + 2H_2(g) \rightarrow HCHO(g) + H_2O(l)$	(2)	−11.7	+46.6	[125]
$CO_2(g) + 3H_2(g) \rightarrow CH_3OH(l) + H_2O(l)$	(3)	−137.8	−10.7	[125]
$CH_4(g) + 0.5\,O_2(g) \rightarrow CO(g) + 2H_2(g)$	(4)	−36.0	−173.0	[126]
$CH_4(g) + H_2O(g) \rightarrow CO(g) + 3H_2(g)$	(5)	+206.0	+142.0	[127]
$CH_4(g) + CO_2(g) \rightarrow 2CO(g) + 2H_2(g)$	(6)	+247.0	+171.0	[127]

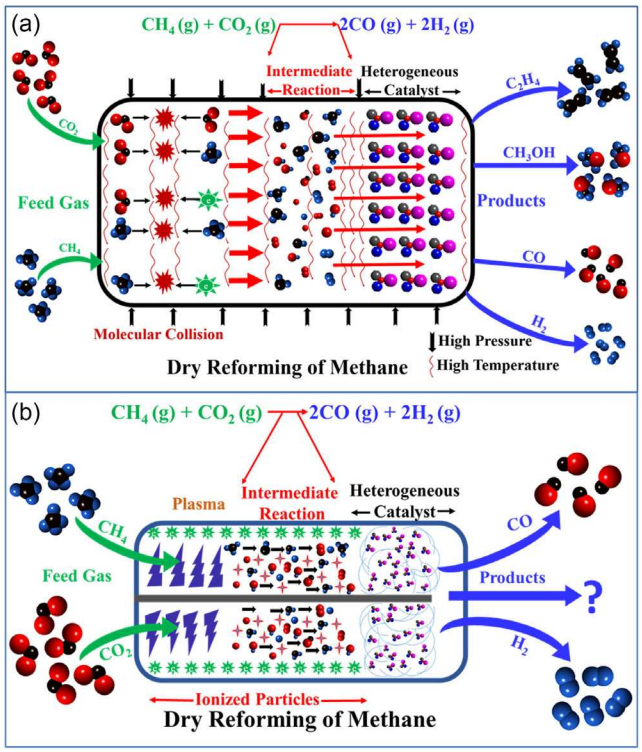

Figure 1. Schematic comparison of DRM reactions in a) thermal catalytic reactor and b) plasma-assisted catalytic reactor.

potential in conversion and efficiency.[52–54] In plasma catalysis, the plasma activation of CH_4 and CO_2 plays a dominant role, with electron impact dissociation serving as the key mechanism to initiate the activation of the DRM reaction.[55] The dissociation energy for CH_4 and CO_2 is 4.5 eV (434 kJ mol^{-1}) and 5.5 eV (532 kJ mol^{-1}), respectively.[46] In plasma catalysis, it has also been reported that the conversion rate of CH_4 is higher than that of CO_2 in the low-temperature range, due to the low dissociation energy of CH_4.[56,57] On the other hand, plasma-only DRM (without heating) is inefficient due to the high activation energy needed for the electron impact process.

The synergy effect of plasma catalysis can significantly enhance the energy efficiency of methane reforming. In comparison, it was reported that the synergy effect in plasma-assited catalysis resulted in a 50% increase in H_2 production and an 80% increase in CO production, compared to the same reaction conducted under thermal catalysis conditions.[58] Such plasma-catalysis synergy is also crucial for enabling low-temperature DRM or other catalytical reactions. For instance, plasma-assisted methane reduction using NiO catalyst was performed at 330 °C, and 37% CH_4 conversion with 99% H_2 selectivity was obtained. Without plasma, only minimal conversion was achieved, however, plasma alone could not initiate the reduction process.[59]

In addition to reforming, plasma catalysis has proven effective in pollutant reduction, achieving a 65% destruction of toluene at 25 °C. This performance significantly outperforms thermal catalysis alone, which achieves less than 10% destruction.[60] Moreover, coke formation due to CH_4 decomposition in thermal catalysis can also be mitigated due to the low operating temperature of the plasma reactor. The molecular excitation and bond breakage due to the introduction of plasma can reduce the coking formed on the catalyst surface from the CH_4 decomposition reaction. Additionally, the deposited carbon on the catalyst surface reacts with CO_2, making CO, $CO_2 + C \rightleftharpoons 2CO$.[61] The carbon oxidation reaction, induced by plasma excitation, occurs at a faster rate compared to that under thermal catalyisis of DRM. Overall, plasma-catalysis synergy is a very promising and efficient way for CH_4 and CO_2 conversion.

4. Critical Performance Parameters for CO_2 and CH_4 Conversion

For thermal or plasma-assisted catalytic conversion reactions, the performance is generally defined by the following terms: conversion rate, efficiency, selectivity, and yield. Most reactor and catalyst designs have been performed to improve these parameters. For a DRM reaction (Equation (6) in Table 1), these terms are represented by the equations given below.

4.1. Conversion Rate

The conversion rate defines the molar ratio of how much the reactant is converted according to the input. The conversion rate of CH_4 and CO_2 in the above equation can be calculated as follows

$$C_{CH_4} = \frac{\text{Moles of } CH_4 \text{ Converted}}{\text{Moles of } CH_4 \text{ Input}} \times 100\% \quad (7)$$

$$C_{CO_2} = \frac{\text{Moles of } CO_2 \text{ Converted}}{\text{Moles of } CO_2 \text{ Input}} \times 100\% \quad (8)$$

4.2. Yield

The yield of a reaction is the ratio of the desired product formed (in moles) to the total amount that could have been made (if the conversion of limiting reactant is 100% and no side reaction occurs). The yield of H_2 and CO of DRM reaction given in Equation (9) and (10) are represented by the following equations

$$Y_{H_2}(\%) = \frac{\text{Moles of } H_2 \text{ Produced}}{2 \times \text{Moles of } CH_4 \text{ Input}} \times 100\% \quad (9)$$

$$Y_{CO}(\%) = \frac{\text{Moles of CO Produced}}{\text{Moles of } CH_4 \text{ Input} + \text{ Moles of } CO_2 \text{ Input}} \times 100\% \quad (10)$$

4.3. Selectivity

The selectivity of a reaction is the ratio of the desired product formed (in moles) to the undesired product formed (in moles). The equation represents the selectivity of H_2 and CO of DRM reaction

$$S_{H_2}(\%) = \frac{\text{Moles of } H_2 \text{ Produced}}{2 \times \text{Moles of } CH_4 \text{ Converted}} \times 100\% \quad (11)$$

$$S_{CO}(\%) = \frac{\text{Moles of CO Produced}}{\text{Moles of } CH_4 \text{ Converted} + \text{Moles of } CO_2 \text{ Converted}} \times 100\% \quad (12)$$

4.4. Efficiency

The energy efficiency of a plasma-assisted catalytic reactor is defined by the conversion of gas (in moles) per unit of plasma power.

$$E(\text{mol J}^{-1}) = \frac{\text{Moles of } (CH_4 \text{ Converted} + CO_2 \text{ Converted})}{\text{Power}} \times 100\% \quad (13)$$

Besides, another energy efficiency formula can also be used in plasma conversion experiments based on specific energy input (SEI) and reaction enthalpy by the following equation

$$\eta_{CO_2} = C_{CO_2} \times \frac{\Delta H^o \text{ (ev. molecule}^{-1})}{\text{SEI (ev. molecule}^{-1})} \quad (14)$$

Here, SEI is the ratio of plasma power and total flow rate, C_{CO_2} is the CO_2 conversion, and ΔH^o is the reaction enthalpy.

5. Nonthermal Plasma Reactors for CO_2 and CH_4 Conversion

Plasma technology has triggered a vast amount of innovative scientific research focused on the nonoxidative conversion of CH_4 and CO_2 to overcome some of the thermal catalytic conversion's thermodynamic and kinetic limitations.[62] A key aspect of plasma technology compared to others is that it can activate and/or dissociate gas molecules at low temperatures by electronic excitation rather than heat[63] or chemical techniques, as shown in **Figure 2**a. Besides, plasma is very flexible, which can be controlled by switching the electricity ON or OFF, and is easy to generate with low maintenance cost.[64]

For non-thermal plasma (NTP) generation in plasma-assisted catalytic reactors, primary considerations in reactor design and configuration include electrode configuration for the electric field, the dielectric barrier to limit discharge current, avoiding thermalization using AC power supply, and gas flow rate to improve convective heat transfer. The efficacy of gas conversion processes, particularly for specific gaseous species, can strongly depend on the reactor type/configuration, as listed in Figure 2b. For instance, the performance of CH_4 conversion into higher hydrocarbons using different plasma sources (DBD, MW, GAP) was studied by Heijkers et al.[65] via a chemical kinetics

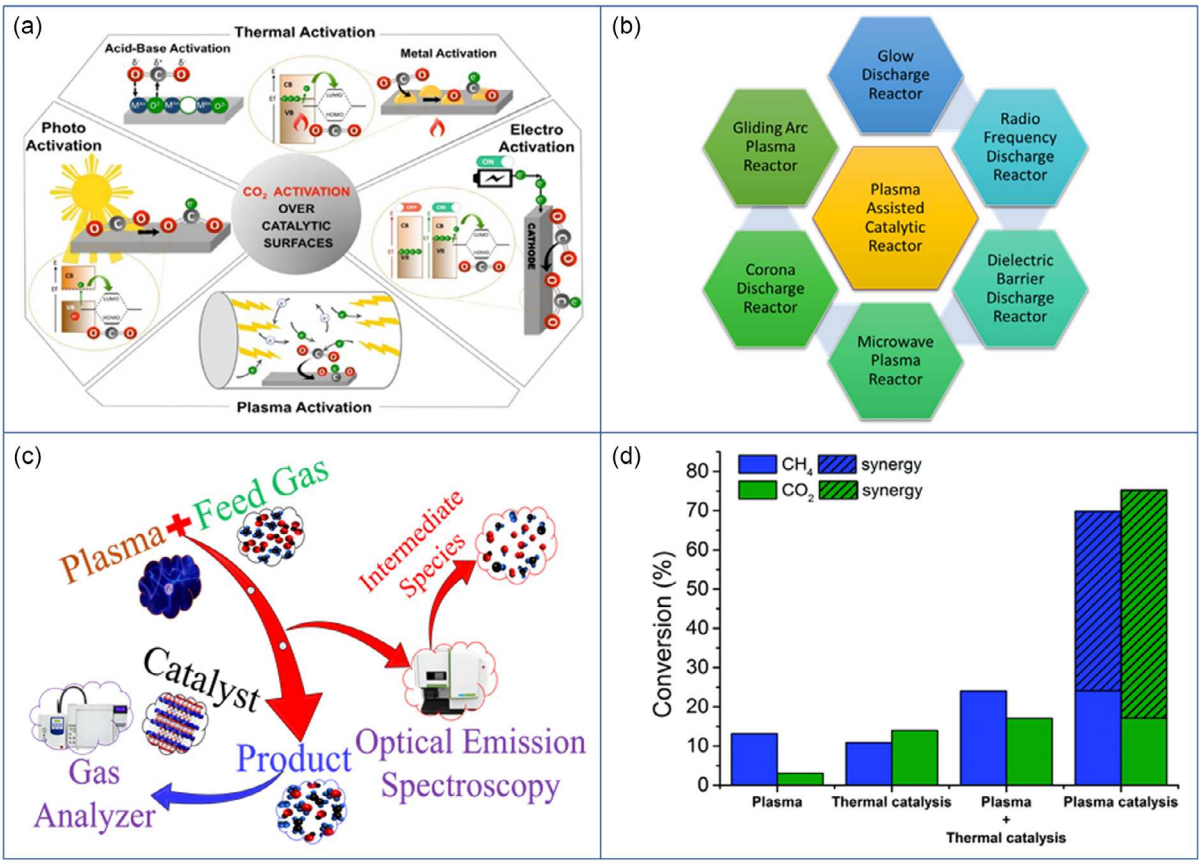

Figure 2. a) Multiple methods of catalytic reaction mechanism. Reproduced with permission.[124] Copyright 2017, Wiley. b) common plasma-assisted catalytic reactors for CH_4 and CO_2 reforming; c) pictorial representation of a plasma-assisted catalytic operation; and d) comparison of CH_4 and CO_2 conversion rate of thermal and plasma-assisted catalysis. Reproduced with permission.[64] Copyright 2017, Royal Society of Chemistry.

model. The simulation results were in reasonably good agreement with the experimental data. They reported 20% CH_4 conversion for the DBD reactor, 80% for the pulsed MW plasma reactor, and 50% for the GAP reactor. In their report, atmospheric pressure MW plasma and GAP result in significantly higher CH_4 conversion than DBD. Also, GAP operates at high flow rates, which is beneficial for higher and more energy-efficient CH_4 conversion. Besides, it has superior selective production because it can operate at a much lower SEI than the other plasma sources (GAP: 1.3 kJ L^{-1}, MW: 24–240 kJ L^{-1}, and DBD: 9–54 kJ L^{-1}). Also, they found negligible vibrational–translational nonequilibrium in all CH_4 plasma-assisted catalytic reactors.

In a separate study, Moss et al.[66] reported the chemical splitting of CO_2 in a pulsed CD from the experimental and numerical simulation. According to their report, for high voltage nanosecond pulses with the mixture of CO_2 and Ar as the feed gases, they found that the shape of pulses leads to two phases of CO_2 splitting. The first phase is dominated by ionization, which promotes a high electron density, and the second phase contributes to a large portion of CO production by direct electron impact dissociation of CO_2. They reported a conversion rate of ≈14% as the best result, which was achieved in a gas mixture of 10% CO_2 – 90% Ar. Compared to other plasma-assisted catalytic reactors, like DBD and MW, they observed that the best energy efficiency (≈80%) was achieved for CO_2 and Ar in the ratio of 1:1 due to the specific form of the applied voltage waveform and its short duration. Besides, the generated energy with plasma was delivered in high-intensity bursts of nanosecond duration in a pulsed CD, thus avoiding the need for long residence times to achieve similar conversion.

The above studies show that the GAP configuration excels in converting CH_4 to higher hydrocarbons, and the CD configuration is best for CO_2 splitting. In contrast, the DBD configuration performs better in the DRM reaction, converting both CH_4 and CO_2 simultaneously. Several studies have investigated optimizing DBD configurations to achieve higher conversion rates and efficiency. Various reactor parameters affecting DBD reactor performance are discussed in detail later. However, the most critical step of DBD plasma-assisted catalytic conversion is gas molecule breakdown, which requires a suitable electrode configuration, power source, and operational gas.[67] Different electrode configurations lead to various types of DBD reactors, with the efficiency of a particular reaction being directly linked to the specific configuration chosen. For instance, adding $BaTiO_3$ packing material shifted discharge characteristics from filamentary to surface discharge for CO_2 conversion reaction.[68,69] This transition led to doubling the average electric field and mean electron energy within the CO_2 discharge, significantly enhancing the process's overall performance. Overall, the synergistic configuration of plasma assistance with a catalyst offers a unique approach to enhancing performance. Figure 2c illustrates the plasma-assisted catalytic reaction methodology, depicting the reaction steps and process.

This review will only focus on DBD reactor parameter influences on overall plasma catalytic performance, particularly for CH_4 conversion, CO_2 splitting, and DRM reactions. Based on several literatures,[70–74] plasma and catalytic synergism play a crucial role, making the plasma-assisted catalytic route more competitive than the thermal conversion of CH_4 and CO_2. A relative comparison of the plasma–catalyst synergy effect is shown in Figure 2d. **Table 2** summarizes the conversions of synergistic plasma catalysis for CO_2 and CH_4 capture reactions considering the effect of different reaction factors.

6. DBD Reactor

The DBD reactor is a promising plasma-assisted catalytic reactor due to its simple design, low input power, nonequilibrium thermal properties, and the capability to induce physical and chemical reactions within gases at a relatively low gas temperature.[75–77] It typically operates with input AC 1–30 kV voltage and a frequency range of 20–500 kHz. This frequency range is suitable for different power supplies, and ≈20 kHz is favorable because of the higher frequency blockage of current transfer.[78,79] Another approach to generating DBD plasma is using pulse power. Pulsed power can enhance ionization efficiency and plasma stability in some applications by delivering energy in short bursts, which allows for more control over electron density, energy distribution, and discharge uniformity.[80,82] In some gas configurations, this method enables a more efficient transfer of energy to the plasma, often leading to higher conversion rates and selectivity. **Figure 3** illustrates the discharge characteristics, including voltage and current waveforms, for improving indoor air quality using AC-DBD and nanopulsed DBD techniques.[82] This review primarily focuses on analyzing AC-DBD, with additional mentions of differences observed in pulse-DBD for the same application.

The plasma generation depends on the applied voltage that must overcome the breakdown voltage of gases to lose their dielectric properties and act as a conductor. **Figure 4** illustrates a standard DBD reactor design consisting of a power supply (source), a reactor chamber where a dielectric barrier separates both electrodes, and an input–output system for reactant and product gases. Based on the product kinds, an oscilloscope, gas analyzer, and other monitoring and analyzing devices are also included.

In a DBD rector, the dielectric barrier limits the current for microdischarges, and most of the charge deposition occurs on the surface of dielectric materials. The gas breakdown condition is represented by Equation (15), which must be satisfied because plasma generation depends upon the applied voltage. When the applied voltage overcomes the breakdown voltage of the gases, the gases turn into conductors from losing dielectric behavior.[83]

$$1 + \gamma(e^{\alpha d} - 1) = 0 \tag{15}$$

$$e^{\alpha d} = \left(1 - \frac{1}{\gamma}\right) \tag{16}$$

where α is the Townsend coefficient, d is the gap distance, and γ is the secondary electron emission coefficient (Equation (15) and (16)).

From Equation (17), the breakdown voltage can be represented by Paschen derivation

Table 2. Plasma-assisted catalytic performance of CO_2 and CH_4 conversion from literature.

Main reactant	Additional reactant	Product	Reactor type	Condition	Temperature [°C]	Catalyst	Conversion [%]	References
CH_4	CO_2	C_2H_6, CO, CH_3OH, CH_3COOH	DBD	Power: 8 W, flow rate: 40 mL min^{-1}, He: 75%,	100–300	CaO	CO_2: 14–45 CH_4: 20	[128]
	CO_2 H_2O	$C_xH_{2n+}1$–OH, $C_xH_{2n+}1$–COOH	DBD	*P*: 6 W, CH_4/CO_2: 2.3, frequency: 5 kHz, flow Rate: 40 mL min^{-1} (75% of He)	46–50	GW-P-0.00 H_2O	CH_4: 22.83 CO_2: 15.81	[129]
	CO_2	H_2, CO	DBD	Power: 45 W, voltage: 30 kV, frequency: 5–12 kHz, flow rate: 50 mL min^{-1}	270	NiC^{700}	CH_4: 65.7 CO_2: 64.6	[130]
	CO_2	CH_3, CH_3OH, CH_3COOH	DBD	Voltage: 5.5 kV, frequency: 3 kHz, flow rate: 30 mL min^{-1} CH_4/CO_2: 2,	55–65	CO/SiO_2	CO_2: 37 CH_4: 49	[131]
						Fe/SiO_2	CO_2: 40 CH_4: 46	
CO_2		O_2, CO	DBD	Voltage: 10 kV, frequency: 50 Hz, flow rate: 15–60 mL min^{-1}	<150	$BaTiO_3$	38.3	[132]
		O_2, CO	DBD	Power: 100 W, frequency: 23.5 kHz, flow rate: 50mL min^{-1}	146	$BaTiO_3$ (bead)	25	[102]
		O_2, CO	DBD	Flow· rate: 50 mL min^{-1}, frequency: 9 kHz, SED: 24–60 kJ L^{-1}		BaTiO3 (bead) SED: 24–60 kJ l^{-1}	28.5	[133]
		O_2, CO	DBD	Voltage: 30 kV, frequency: 5–20 kHz, flow· rate: 25–125 mL min^{-1}		Modified electrode	27.2	[92]
	H_2	CH_4	DBD	Voltage: 9.4 kV, frequency: 1 kHz	260	10 wt% Ni/zeolite	96	[134]
	H_2	CH_4, CO	DBD	Voltage: 13–18 kV, frequency: 40–42.8 kHz, flow rate: 200mL min^{-1} H_2/CO_2: 4:1	120–170	Pre-plasma-treated, $Ce_{0.58}Zr_{0.42}O_2$	80	[135]
	H_2	CH_4, CO	DBD	Voltage:10–15 kV, frequency: 40–41 kHz, flow rate: 200 mL min^{-1}, H_2/CO_2 : 4:1, GHSV: 50 000 mL h^{-1}	80–450	$Ce_xZr_{1-x}O_2$	85	[136]
	H_2	H_2O, CO	DBD	Power: 30 W, flow rate: 36 mL min^{-1}, H_2/CO_2: 3:1, GHSV: 2200 mL h^{-1}	80–240	Pd/ZnO	32.5	[137]

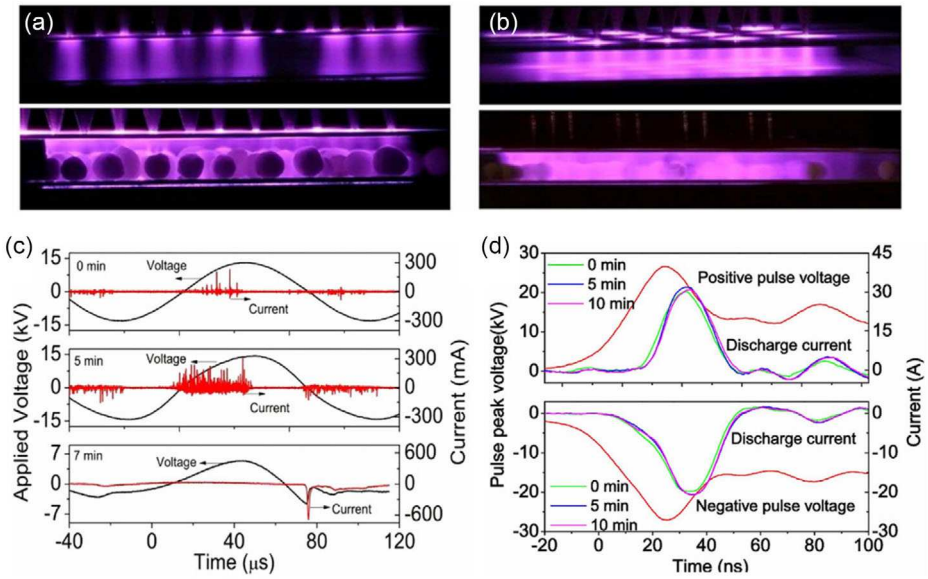

Figure 3. Plasma discharge image of empty (top) and packed bed (bottom) electrode gap a) AC-DBD and b) pulse-DBD; voltage and discharge current of power supply c) AC-DBD and d) pulse-DBD [air quality improvement, gas flow: $N_2 + O_2$]. Reproduced with permission.[82] Copyright 2016, Springer Nature.

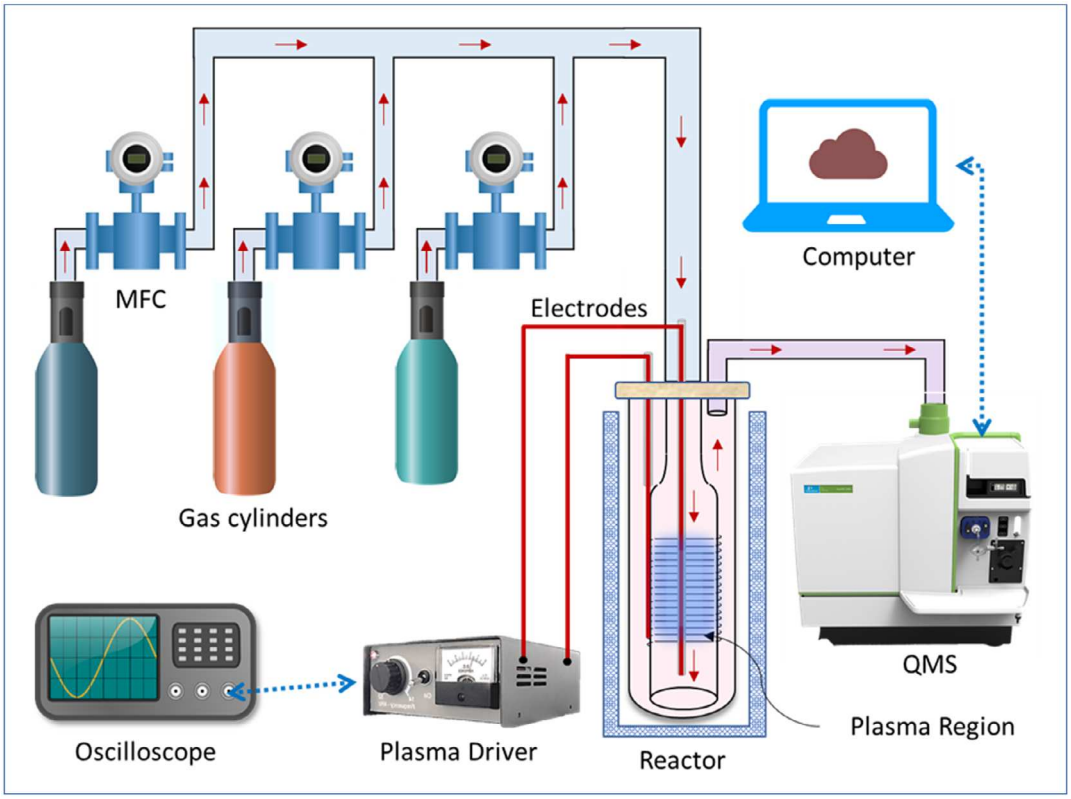

Figure 4. Schematic of a DBD reactor.

$$V_b = \frac{Bpd}{\left[\ln\{Apd - \ln\left(\ln\left(1+\frac{1}{\gamma}\right)\right)\right]} \tag{17}$$

where A and B are the constants calculated by the following formula

$$A = \frac{\sigma_n}{kT_n} \tag{18}$$

where , σ_n means electron–neutral collisional cross section, T_n is the neural atom temperature, and k is the Boltzmann constant.

$B = AV_i$, where V_i is the ionization potential.

DBD reactor configuration varies according to discharge types, such as planar, cylindrical, and surface discharges. Besides, it can generate many microdischarges at atmospheric pressure, which is considered a substantial property ("low" pressure). The microdischarge property depends on the gas mixture, pressure, and electrode configuration. **Table 3** shows the characteristics of the microdischarge properties for a 1 mm air gap at 1 bar.[84]

In addition to traditional DBD configurations, several innovative structures such as water–electrode DBD, multielectrode DBD, water-cooled electrode DBD, and dual DBD (DDBD) reactors have been developed to enhance plasma–catalyst interactions and improve conversion efficiencies.[85–89] Water-electrode DBDs, for example, use water as one of the electrodes, which aids in cooling and stabilizes plasma at higher power levels. This setup reduces electrode erosion, allows for longer operating times, facilitates the removal of reaction by-products, and enables temperature control within the reaction zone, which is particularly advantageous for sensitive catalytic processes.[86] However, the application of water–electrode DBD in CH_4 or CO_2 conversion has been limited.

Water-cooled electrodes offer another means to maintain stable discharge at a consistent initial applied voltage, especially in N_2 environment.[87] Additionally, using multiple electrodes is an approach to control product selectivity and discharge distribution.[89] DDBD reactors, which feature two dielectric barriers between electrodes, produce a more uniform electric field, minimizing the risk of arcing. This uniformity enhances plasma stability and allows for more controlled catalyst interactions.

Table 3. Microdischarge characteristics. Reproduced with permission.[84] Copyright 1997, HAL Open Science.

Duration	1–10 ns
Filament radius	About 0.1 mm
Peak current	0.1 A
Current density	100–1000 A cm^{-2}
Total charges	0.1–10 nC
Electron density	10^{14}–10^{15} cm^{-3}
Electron energy	1–10 eV
Gas temperature	Close to average gas temperature

However, the performance depends on the setup configuration and type of dielectric barrier. Mei et al.[88] compared single and dual DBD (SDBD and DDBD) reactors, finding that the SDBD reactor exhibited a higher electron density and generated more reactive species, resulting in greater CO_2 (24.1%) and CH_4 (49.2%) conversions. However, DDBD achieved higher gaseous product selectivity, while SDBD favored liquid product selectivity.

6.1. Key Design and Operational Parameters

The experimental procedure, target, and characterization parameters are vital in designing a DBD reactor. Mostly two concentric cylindrical electrodes are most often used for gas conversion applications in typical DBD reactor.[90,91] Critical reaction parameters, such as discharge length, discharge gap, discharge power, discharge frequency, dielectric material thickness, and feed flow rate, have been meticulously investigated to fine-tune performance. For instance, Mei et al.[92] developed a regression model to determine the effectivity of each reactor parameter in the CO_2 decomposition/splitting conversion within a cylindrical DBD reactor given in Equation (19)

$$CO_2(g) \rightarrow CO(g) + 0.5\,O_2 \tag{19}$$

According to their report, the significance of processing parameters for conversion and efficiency follows the order: q (feed flow rate) $\approx P$ (discharge power) $> d_g$ (discharge gap) $> L$ (discharge length) $> d_T$ (thickness of dielectric material) $> f$ (discharge frequency) and $P > q > d_g > d_T > L > f$, respectively. Several groups also investigated the effect of power and frequency in a plasma-assisted catalytic gas conversion. According to their findings, it was clear that increasing plasma power increases the electric field, electron density, and electron temperature and increases conversion.[92–94]

Liu et al.[95] conducted a comprehensive investigation into the intricate impact of discharge power, feed flow rate, and frequency on the conversion of CH_4 into H_2 and higher hydrocarbons. They performed the experiment in a coaxial DBD reactor at atmospheric pressure and low temperatures. They also developed a three-layer back-propagation artificial neural network (ANN) simulation model and predicted the selectivity and yield of gas products and the energy efficiency for this complex reaction. Their model predicted that discharge frequency is the least essential parameter for CH_4 conversion in the DBD reactor. Based on their ANN model, **Figure 5** shows the effect of discharge power, feed flow rate, and frequency on the performance parameters (conversion rate, selectivity, and yield) for nonoxidative conversion of CH_4. Figure 5a shows that discharge power plays the most pivotal role in all the performance parameters. For example, a maximum of 36% CH_4 conversion was found for 75 W discharge power. Similarly, H_2 selectivity and yield increase to 44.7% and 40%, respectively. However, C_2H_2 and C_2H_4 selectivity was limited to 30%, while the enhancement of saturated hydrocarbons such as C_2H_6 and C_3H_8 was acheived. The yield of saturated hydrocarbons also increased with the discharge power. Thus, the findings indicate that increasing discharge power promotes the formation of saturated hydrocarbons in the reaction.

In DRM applications, the performance trends observed for changes in plasma power and frequency closely resemble those seen in CH_4 conversion and CO_2 splitting reactions. Snoeckx et al.[96] performed a numerical simulation in a DBD reactor for DRM reaction and concluded that their simulated results agreed with several experimental results. The results revealed the upward conversion trend with increasing plasma power. On the other hand, the frequency was counted as a less critical parameter unless it is a product of resident time ($\tau \cdot f$) and frequency. Zhang's[97] results showed that CH_4 and CO_2 conversion increased with plasma power. They found a 23% increase in CH_4 conversion (17–40%) and a 15% increase in CO_2 conversion (12–27%), respectively, with the increasing power from 25 to 75 W. A similar trend was observed by the experimental observation of Mei et al.[98] for plasma power, but the energy is more related to the feed gas flow rate. In terms of product formation, an increase in H_2 yield and selectivity was also observed with increasing discharge power, leading to higher H_2 production but lower CO production up to a certain threshold.[53] At very high discharge levels, the presence of O' radicals from CO_2 alters the reaction characteristics of the DRM reaction. Increasing plasma power consistently enhances conversion across all three applications (CH_4 conversion, CO_2 splitting, and DRM). However, feed gas flow and catalyst selection significantly influence the desired product formation.

In contrast, frequency plays a critical role in DRM performance within a pulse-DBD reactor, as it increases discharge over the residence time. Wang et al.[99] studied the DRM reaction at room temperature with a total gas flow rate of 50 sccm, finding that conversions increased with higher pulse repetition frequency (PRF). Maximum conversion rates of 39.6% for CH_4 and 22.9% for CO_2 were achieved at a pulse frequency of 10 kHz with a discharge power of 55.7 W. Additionally, shorter rise and fall times enhanced energy conversion due to the rapid acceleration of electrons within the shortened discharge time. From a kinetic perspective, the increased conversion with PRF, resulting in CO and H_2 generation, is attributed to the electron impact dissociation of CO_2 and CH_4.[100]

In the feed gas effect, the CH_4 conversion decreased with the increasing flow rate up to 300 mL min^{-1} with a minimum value of 8% due to the low residence time, as shown in Figure 5b. The yield of H_2 followed a similar trend to the CH_4 conversion, which decreased from 8.9% to 1.6% for the flow rate from 50 to 300 mL min^{-1}. Besides, the C_3 and C_4 (hydrocarbon) selectivity decreased by three times with the upward flow rate. However, the selectivity of C_2 hydrocarbons showed a notable rising trend. Conversely, in DRM reactions, a higher feed gas flow rate hinders CH_4 and CO_2 conversion while increasing CO selectivity and decreasing H_2 selectivity.[53] The presence of CO_2 in the DRM environment may accelerate the reverse water gas shift reaction process.

The excitation frequency was found to be the least essential parameter described previously for AC-DBD. In Figure 5c, a change in frequency from 20 to 70 kHz resulted in a slight 6% decrease in CH_4 conversion. Similar results were also noticed for H_2 yield and selectivity, while hydrocarbons' selectivity and yield (C_2–C_4) were almost independent of frequency.[95] In another study, Mei et al.[92] found almost a 5% decrease in the conversion of CO_2 and energy efficiency when increasing the discharge frequency from 8 to 11 kHz at a constant SEI of 96 kJ L^{-1}. A similar trend was observed in the CO_2 splitting

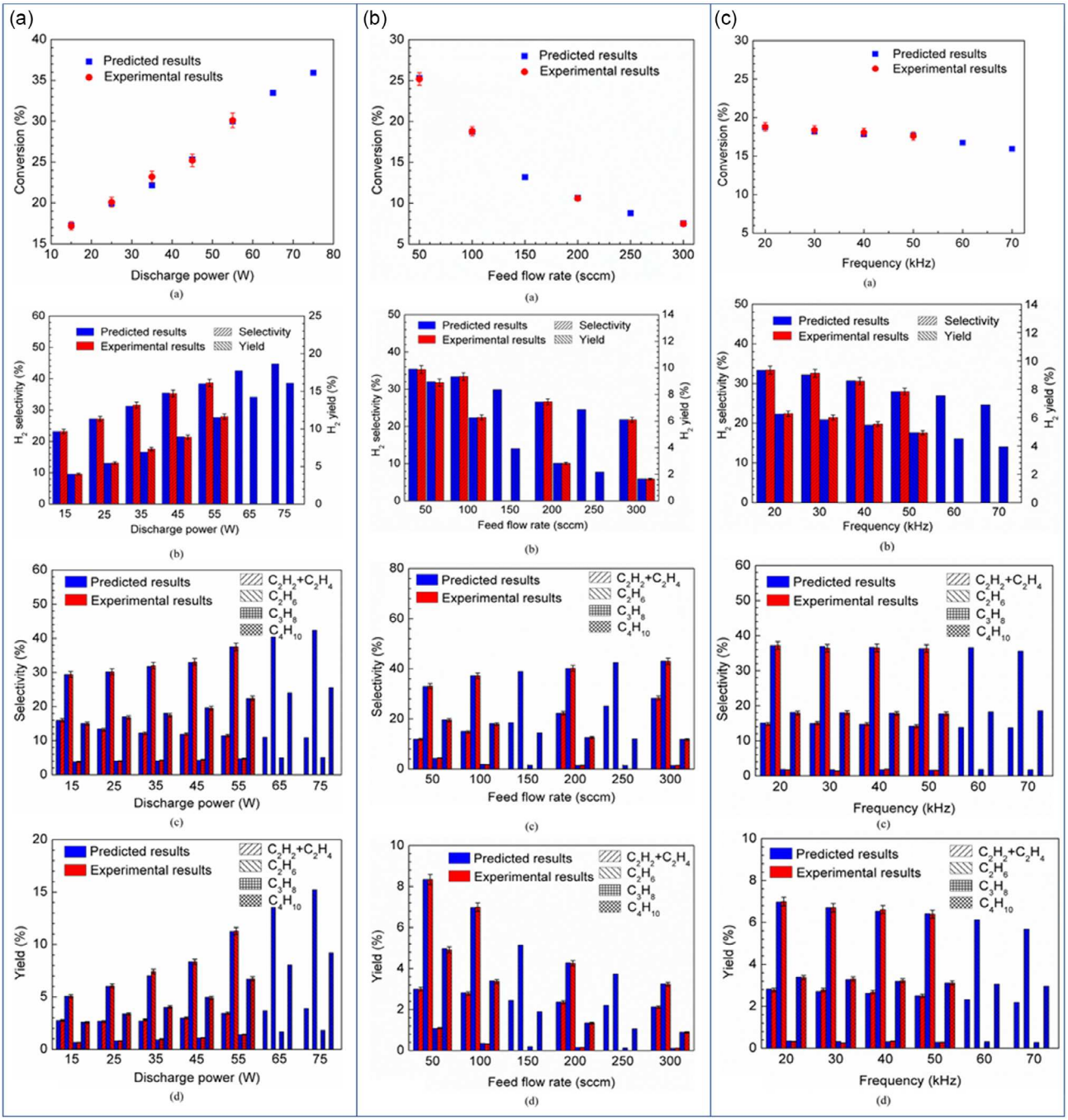

Figure 5. Effect of a) discharge power; b) feed flow rate; and c) frequency on the conversion rate, selectivity, and yield of nonoxidative conversion of CH_4 and energy efficiency. Reproduced with permission.[95] Copyright 2014, American Chemical Society.

reaction, with conversion decreasing from 22.0% to 17.5% and energy efficiency decreasing from 15.3% to 12.5% as the frequency increased from 16.2 to 28.6 kHz. This decrease is attributed to a drop in gas voltage at higher frequencies.[94] Similar results were also predicted by Snoeckx et al.[96] for DRM application, where the model found the exact maximum conversions and energy efficiencies for all gas mixtures, either for the residence time (τ) of 100 s and a frequency (f) of 10 kHz, or the residence time of 10 s and a frequency of 100 kHz. They also reported a sharp decrease in the conversion rate and energy efficiencies for the frequency of 100 kHz and a residence time of 100 s. Thus, they concluded that the product of both frequency and residence time ($\tau \cdot f$), which was the total number of microdischarge filaments experienced by gas molecules in the reactor vessel, was more important rather than the frequency and residence time individually. The feed gas mixture ratio significantly affects

performance in DRM applications. Our previous experimental study[53] found that a higher CO_2 proportion in the feed gas mixture enhances conversion and efficiency. This was corroborated by another experiment and simulation model,[96] which reported excellent agreement on the influence of the CO_2 and CH_4 gas mixture ratio. The model showed that a higher CO_2 concentration substantially improves both the conversion rate and efficiency. However, the trends in product formation become more complex when the feed gas mixture ratio is varied.[53,101]

The discussion on discharge power, feed gas flow rate, and discharge frequency concludes that discharge power increases conversion across all reaction types, including CH_4 conversion, CO_2 splitting, and DRM reaction. Higher feed gas flow rates decrease conversion in all cases, while discharge frequency has minimal impact on reactions, particularly for DRM.

Another crucial factor in plasma catalysis is the bed material, which serves as a dielectric material and influences the reaction through microdischarges. The effect of these microdischarges varies depending on the specific reaction. Michielsen et al.[102] investigated the effect of bed material on the CO_2 dissociation reaction. Their experimental results showed a positive impact on conversion rate and energy efficiency (25% and 4.5%, respectively) when $BaTiO_3$ was used as the bed material in the reactor. Mei et al.[69] found a similar trend of 29% conversion and 0.25 mmol kJ^{-1} energy efficiency for similar bed materials and applications. According to their theory, this was due to the higher dielectric constant of $BaTiO_3$ ($\varepsilon \approx 4000$), which results in an enhanced electric field and lower breakdown voltages. Besides space and increasing contact points, it also supports electric field enhancement. Another study of dielectric materials was performed by Li et al.[103] for plasma-assisted catalytic CO_2 decomposition with three different dielectric materials as barrier $Ca_{0.7}Sr_{0.3}TiO_3$, alumina, and silica. They reported a higher conversion rate of 15.6% for $Ca_{0.7}Sr_{0.3}TiO_3$ with 0.5 wt% $Li_2Si_2O_5$. However, in the case of DRM reactions, $BaTiO_3$ negatively affected conversion due to the presence of CH_4. In a separate study on the impact of bed material on DRM, Michielsen et al.[104] found that $BaTiO_3$ led to increased production of oxygenated products, which adversely affected the selectivity of desired products. In contrast, α-Al_2O_3 with a particle size of 2.0–2.24 mm yielded the highest conversions, achieving 33% for CH_4 and 23% for CO_2. It is known that the polarity of the electrodes changes for AC voltage, which generates microdischarges of nanosecond duration. These microdischarges randomly appear at every half-cycle and reform at the breakdown voltage, and then reach the next half-cycle of voltage. Thus, continuous microdischarges formed twice the applied frequency and appeared as spikes. Although it looks like microdischarges are distributed randomly on the dielectric surface, the actual position depends on residual distribution on the dielectric surface and the dielectric constant of the barrier.

The influence of the discharge gap/dielectric barrier thickness (the distance between the high-voltage and grounded electrodes) has also been extensively studied. Notably, the optimal discharge gap is linked to the choice of catalysts, packing material, feed gas composition, and applied voltage. Kostov et al.[105] explored the impact of the discharge gap on plasma performance. In their study, where electrodes were covered by two glass slabs, they identified an optimal discharge gap of 1.5 mm of air for maximizing discharge power, reaching up to 3 W at 20 kV. This finding was further validated and supported through the analysis of Lissajous figures. Ozkan et al.[106] investigated dielectric barrier thickness for CO_2 splitting reaction and reported higher CO_2 conversion of up to 50% for large dielectric barrier thicknesses, ranging from 2.0 to 2.8 mm. The best results were obtained at an absorbed power of 70 W (corresponding to an SEI of 5.75 eV per molecule), the largest dielectric thickness (2.8 mm), 17% conversion, and 9% energy efficiency. It is also reported that smaller space or discharge gaps promote more vital electric fields and achieve greater conversion rate and selectivity.[102,107–110] Delikonstantis et al.[111] reported that selectivity decreased with increasing discharge gap and concluded that maximum energy input into the discharge is reached with an optimum discharge gap. In his report, the 2.5–3.5 mm discharge gap achieved higher selectivity of C_2H_2 for CH_4 conversion. A similar conversion and discharge gap relation was also reported by Uytdenouwen et al.[112] where CO_2 dissociation increases from 10% to 30% by decreasing the gap size from 4.7 to 1.2 mm. Therefore, determining the optimal discharge gap/thickness is not straightforward, as it is heavily influenced by other reaction parameters. However, generally speaking, a smaller gap tends to increase conversion.

Similar to other reactor parameters, the shape and size of the electrode also play a significant role in influencing the discharge pattern and, consequently, the reaction process in some cases. A study by Mei et al.[92] has shown that the modified electrode positively impacts CO_2 conversion. Their results showed that the maximum energy efficiency of 10.4% and CO_2 conversion of 20.0% were achieved with a combination of Al foil outer electrode and stainless steel (SS) screw-type inner electrode when plasma power was 10 W, and the CO_2 flow rate was 50 mL min^{-1}. They maintained that the sharp edge of the SS screw-type electrode distorts the electric field in the discharge region, i.e., enhancing the local electric field near the inner electrode and generating more intensified filaments near the sharp edge of the screw electrode. Thus, more reaction channels could be generated, significantly contributing to enhanced performance. The contribution was evidenced by the increase in the number and amplitude of the current pulses.

6.2. Minor Reaction Variables

Adjusting other electrical properties in the DBD plasma process slightly alters the discharge pattern but does not significantly impact the reaction process. For instance, electric pulse polarity and pulse power were analyzed by Lee et al.[104] for DRM reaction, and bipolar pulse power was more effective than the unipolar pulse. However, the selectivity of the product was not affected by the pulse polarity. The effect of the waveform shape is considered less important in plasma-assisted catalytic gas conversion and efficiency, as reported by Brock.[113] Because the waveform shape effect can only control the percentage of plasma time in the reactor, plasma will go through the typical glow region after attaining the breakdown voltage. However, they mentioned square > sine > triangular, an order based on attaining faster breakdown voltage, resulting in a larger relative percentage of time per cycle, i.e., a more extended plasma environment.

However, high efficiency followed the order of triangular > sine > square. Song et al.[114] also reported a similar result, where pulsed plasma enhanced the conversion rate in a cylindrical DBD reactor for DRM reaction. The influence of diluent gases on plasma-assisted catalytic conversion of CO_2 and CH_4 also showed positive results in conversion and efficiency. Ray et al.[115] tested three diluent gases, nitrogen (N_2), helium (He), and argon (Ar), for CO_2 decomposition. They reported that Ar played a significant role with a maximum CO_2 conversion of 19.5% in a packed DBD reactor with a CO_2:Ar ratio of 1:2. The best CO yield (16.8%) was also obtained under the same conditions and the highest energy efficiency at 0.945 mmol kJ^{-1}. A similar observation was reported by Nguyen et al.[116] and Brock et al.[117] where they assume diluent gas affects facile energy transfer from metastable species to CO_2 molecules. Adding He as a diluent gas affects the CO_2 dissociation. The following electron impact and dissociation may be responsible for adding He.[118]

$$He + e^- \rightarrow He^* + e^- \quad (20)$$

$$He^* + CO_2 \rightarrow He + CO + O \quad (21)$$

The aforementioned reaction parameters have a relatively minor influence on catalysis reactions.

6.3. Surface Reaction Role in Product Selectivity

In addition to plasma reactor parameters, the interaction of plasma with the catalyst surface controls reaction pathways through surface reaction toward desired product formation. For instance, Vakili R et al.[22] studied the DRM reaction with and without catalysts, revealing through in situ analysis how surface reactions can alter selectivity. **Figure 6** represents an in situ diffuse reflectance infrared Fourier transform spectroscopy (DRIFTS) characterization to understand the gas–solid surface interaction when the feed gas was exposed to the as-prepared Pt nanoparticle on UiO-67 metal–organic framework (PtNP@UiO-67) catalyst to perform a DRM reaction in a DBD reactor. In Figure 6a, the CH_4 and CO_2 adsorption peaks can be seen at the 3015 and 2360 cm^{-1} band, respectively, during the plasma-OFF condition. During the plasma-ON condition, various surface species, including monodentate and bidentate carbonates at 1515 and 1550 cm^{-1}, were observed for the adsorption of CO_2 on the UiO-67 surface. In Figure 6b, with time, CO adsorption on the metallic catalyst was noticed from a broad peak ranging from 1900 to 2100 cm^{-1}, as well as other CO adsorption peaks were also noticed, such as at 2115 and 2150 cm^{-1}. These peaks represent the DRM reaction progress. New vibrational bands at 1590 and 1550 cm^{-1} were observed after 1 min of the plasma ignition, indicating formates and carbonates, respectively, shown in Figure 6c. This is because of adsorbed CO_2 on the surface undergoes a series of transformations, forming carbonates (CO_3^{2-}), which then convert to formates (HCO_2^-) and ultimately to CO and OH on Pt NPs. After 5 min, the formates, carbonates, and CO concentrations stabilized, indicating that the DRM reaction reached a steady state. The decomposition of formates on metallic Pt NPs subsequently leads to C_2H_2 through the dehydrogenation of C_2H_4, as evidenced by peaks at 1415 and 1610 cm^{-1} in the spectral analysis. These results underscore the dynamic interplay between plasma and catalyst

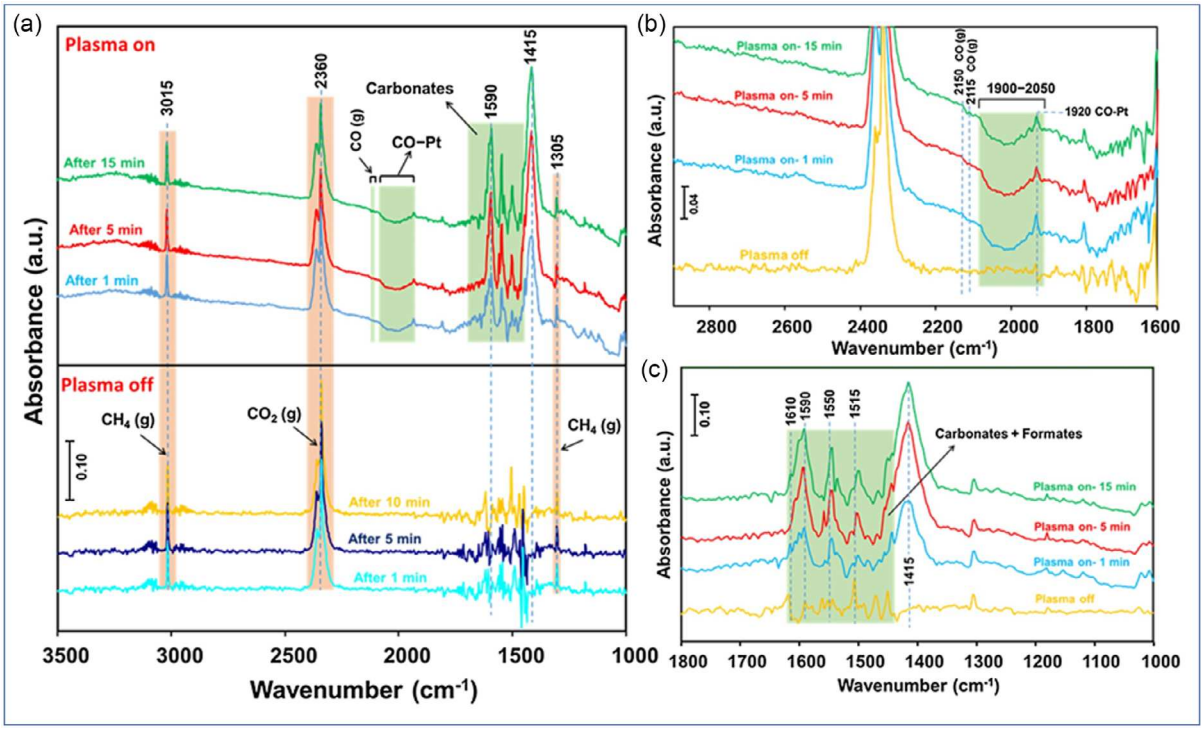

Figure 6. In situ DRIFTS spectra to show surface interaction of absorbed and formation of carbon species in DBD plasma reactor. a) whole adsorbed species, b) CO adsorbed, and c) carbonates and formates adsorbed on PtNP@UiO-67 catalyst during plasma-assisted DRM. Reproduced with permission.[22] Copyright 2020, Elsevier.

surface reactions in influencing product selectivity. This type of reaction, such as C_2H_2 formation on the catalyst surface, was not observed in the absence of a catalyst in their study, highlighting the synergistic effect of plasma and catalyst interaction with the influence of surface reactions.

The DBD reactor exhibits potential as a plasma-assisted catalytic reactor due to its straightforward design, low input power requirements, and capacity to facilitate physical and chemical reactions at comparatively low gas temperatures. The reactor operates with input AC voltage and frequency, and the breakdown voltage of gases must be overcome for plasma generation. Various reactor parameters such as discharge power, feed flow rate, discharge gap, and frequency influence DRM, CH_4 conversion, and CO_2 splitting conversion and efficiency. The choice of dielectric material and electrode configuration can also impact reactor performance. Diluent gases, waveform shape, and electrode polarity are additional factors affecting the conversion and efficiency of plasma-assisted catalytic reactions. Understanding these parameters and their interactions can lead to the rational engineering of DBD reactors for more efficient and sustainable chemical conversions.

7. DBD Plasma Process Inefficiency and Challenges in Catalysis

In any catalysis research work, energy efficiency is always the primary concern. The loss of energy must be minimized to improve efficiency. In plasma-assisted catalytic reactions, power loss as heat during high voltage transformation is a significant issue for plasma-catalysis energy efficiency. Sadat et al.[119] developed a model for calculating the heat loss of a DBD reactor based on which they reported that heat is generated in a DBD reactor by elastic collisions and lost by conduction across the gas layer and the composite envelope of the reactor. They used electrode temperature measurements and found 86% input power dissipation to the environment by convection and radiative heat transfer for He and 42% for air as flowing gas. This power dissipation can be attributed to the gas's nature, which can be decreased with increasing input power.

Table 4 represents the energy balance over a steam-reforming DBD reactor by Kappes et al.[120] They summarize that more than 60% of the electrical energy input is spent on heating the dielectric barrier because most plasma energy spent on dissociating CH_4 is re-emitted as heat during the recombination of the intermediate species. On the other hand, more than 50% of the plasma energy is absorbed by the vibrational excitation of H_2O and CH_4 and does not contribute substantially to forming the desired reaction products. Thus, it requires higher mean electron energy than it is obtained in DBD. Increasing the ratio of dissociative collisions to vibrational excitation was suggested to be efficient activation.

Besides power loss during electrode heating, temperature could affect the discharge properties in plasma-assisted catalytic reactions, as illustrated in **Figure 7**a,b. Zhang et al.[121] reported the discharge properties of the DBD reactor by *V–I* waveform and Lissajous diagrams with fixed discharge power $P_{dis} = 10$ W and $U_{peak} = 10$ kV for five different temperatures: 297, 473, 673, 773, and 873 K. According to his report, the discharge properties showed the increased intensity of filamentary microdischarge with increased temperature up to 673 K. Figure 7a shows that the Lissajous diagram maintains a smooth parallelogram up to temperature $T = 773$ K. However, at $T = 873$ K, the Lissajous diagram lost shape and concluded the absence of typical microdischarge. The voltage–current waveform or *V–I* waveform also represented a similar conclusion. For $T = 773$ K, the discharge intensity decreased significantly compared to $T = 673$ K, as shown in Figure 7b. The electrical properties are also enhanced by increasing the duty cycle,[122] as demonstrated in Figure 7c. It is clear from Figure 7c that the number of pulses and amplitude for voltage and current improved at positive and negative cycles, increasing the duty cycle from 10% to 40%. These *V–I* profiles later demonstrated the microdischarge properties in plasma-assisted catalytic reactions.

Low-temperature operation is a key advantage of plasma-assisted catalytic reactors, but maintaining room temperature with a suitable plasma–catalyst combination remains a significant challenge. Extensive research is underway to identify catalysts compatible with various plasma-catalysis applications, as resolving this challenge would dramatically boost reactor efficiency. A clear understanding of the interactions between different excited states, such as electronic or vibrational excitation of particles with a plasma source, and their impact on product formation is also crucial. Understanding the specific plasma mechanisms for different gas species and catalysts is an ongoing area of research. Additionally, maximizing energy efficiency and minimizing energy loss are crucial objectives in catalysis research, as they directly contribute to improved overall productivity.

To optimize and control DBD plasma for catalytic reactions, it is crucial to diagnose and understand key plasma parameters such as electron energy, electron density, and gas temperature. These parameters are pivotal in defining reaction pathways

Table 4. Energy balance over a steam-reforming DBD reactor. Reproduced with permission.[120] Copyright 2002, IAEA Scientific.

Energy sources		Energy sinks	
The heat of the incoming gas	30 W	The heat of outgoing gas	−17 W
Plasma power	180 W	Reaction enthalpy	−5 W
Electrical heating	80 W	Heating of the barrier	−113 W
–	–	Heat loss to the environment	−93 W
–	–	Rest (such as heating of caps and electrodes)	−62 W
–	290 W	–	−290 W

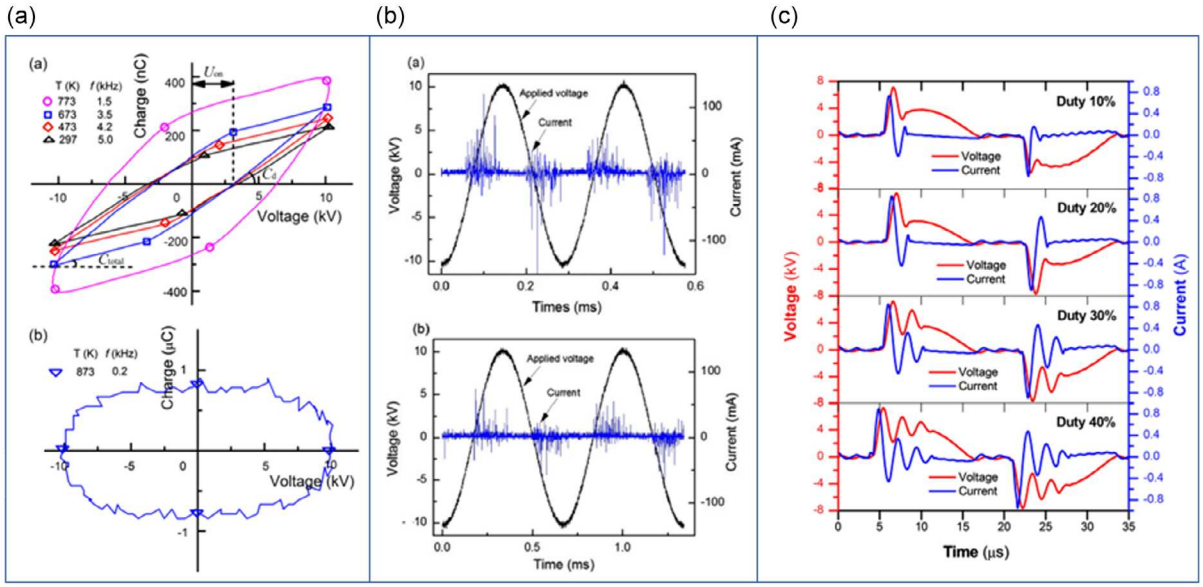

Figure 7. a) Typical *V–Q* Lissajous diagrams with various temperatures: 297, 473, 673, 773, and 873 K. Reproduced with permission.[121] Copyright 2013, Institute of Physics. b) typical voltage and current waveforms at 673 and 773 K. Reproduced with permission.[121] Copyright 2013, Institute of Physics, and c) voltage and current waveforms under various duty cycles. Reproduced with permission.[122] Copyright 2020, Elsevier.

and selectivity for products in plasma–catalytic reactions. Electron energy distribution affects the ionization potential and the energy available for bond dissociation, thus influencing reaction rates and selectivity. For instance, higher electron energy can favor CH_4 dissociation and subsequent formation of C_2 hydrocarbons, while moderate energies are often preferable for selective CO_2 splitting. Electron density, which impacts the concentration of reactive species, can be measured using techniques like Langmuir probes and MW interferometry.[123] Additionally, gas temperature, typically evaluated through optical emission spectroscopy, plays a critical role in stabilizing plasma and minimizing thermal effects that might deactivate the catalyst. Controlled manipulation of these plasma parameters has been shown to optimize conversion efficiency and improve the selectivity of products in plasma-assisted catalysis.

In conclusion, the mechanism of plasma catalysis is influenced by a multitude of factors, including reactor type, size, design, input species, temperature, and catalyst morphology. Further research is necessary to fully elucidate the intricacies of plasma-assisted thermal catalysis across various reactor configurations.

8. Summary

This review comprehensively analyzes the design parameters of DBD plasma-assisted catalytic reactors for CH_4 and CO_2 conversion. The DBD reactor is preferred for plasma catalysis due to its simple configuration, cost-effectiveness, and superior performance. DBD plasma generates various ionized particles with the reactants during the reaction, leading to numerous intermediate reactions and product formation. However, the underlying mechanism remains unclear and requires further investigation to establish a comprehensive theory. The catalyst and reactor design parameters such as voltage, frequency, dielectric material, electrode gap size, and gas flow influence the reaction mechanism and performance. Specific reactor designs are necessary to achieve the desired selectivity for particular reactions, including CH_4 conversion, CO_2 splitting, and DRM reaction.

Acknowledgements

This project was supported by grants from the National Science Foundation (CBET 2427238 and TI 2427213).

Conflict of Interest

The authors declare no conflict of interest.

Keywords

dielectric barrier discharge, dielectric barrier discharge reactors, plasma inefficiency, plasma-catalysis, reactor design parameters

Received: June 15, 2024
Revised: November 4, 2024
Published online: December 6, 2024

[1] A. Stips, D. Maclas, C. Coughlan, E. Garcia-Gorriz, X. S. Liang, E. J. Brook, S. Harder, J. Severinghaus, E. J. Steig, C. M. Sucher, D. Lashof, *Global Biogeochem. Cycles* **2000**, *6*, 559.
[2] Overview | Energy Economics | Home, https://www.bp.com/en/global/corporate/energy-economics/energy-outlook/overview.html (accessed: April 2024).

[3] EDGAR - The Emissions Database for Global Atmospheric Research, https://edgar.jrc.ec.europa.eu/report_2023?vis=co2tot#emissions_table (accessed: April 2024).
[4] Y. Zheng, W. Zhang, Y. Li, J. Chen, B. Yu, J. Wang, L. Zhang, J. Zhang, *Nano Energy* **2017**, *40*, 512.
[5] A. Galadima, O. Muraza, *Renewable Sustainable Energy Rev.* **2019**, *115*, 109333.
[6] D. R. Kauffman, J. Thakkar, R. Siva, C. Matranga, P. R. Ohodnicki, C. Zeng, R. Jin, *ACS Appl. Mater. Interfaces* **2015**, *7*, 15626.
[7] K. Li, B. Peng, T. Peng, *ACS Catal.* **2016**, *6*, 7485.
[8] A. Raksajati, M. T. Ho, D. E. Wiley, *Ind. Eng. Chem. Res.* **2013**, *52*, 16887.
[9] X. Wu, Y. Yu, Z. Qin, Z. Zhang, *Energy Proc.* **2014**, *63*, 1339.
[10] V. Havran, M. P. Duduković, C. S. Lo, *Ind. Eng. Chem. Res.* **2011**, *50*, 7089.
[11] M. Aresta, A. Dibenedetto, *J. Chem. Soc. Dalton Trans.* **2007**, 2975.
[12] M. S. A. Rahaman, L. H. Cheng, X. H. Xu, L. Zhang, H. L. Chen, *Renewable Sustainable Energy Rev.* **2011**, *15*, 4002.
[13] E. I. Koytsoumpa, C. Bergins, E. Kakaras, *J. Supercrit. Fluids* **2018**, *132*, 3.
[14] R. V. Ranganathan, M. Monir Hossain, S. Talukdar, R. Ahasan, R. Wang, M. Uddi, in *2021 IEEE Int. Conf. on Plasma Science (ICOPS)*, IEEE, Lake Tahoe, NV, September **2021**, p. 1, https://doi.org/10.1109/icops36761.2021.9588526.
[15] H. D. Gesser, N. R. Hunter, D. Probawono, *Plasma Chem. Plasma Process.* **1998**, *18*, 241.
[16] X. Tao, F. Qi, Y. Yin, X. Dai, *Int. J. Hydrogen Energy* **2008**, *33*, 1262.
[17] L. M. Zhou, B. Xue, U. Kogelschatz, B. Eliasson, *Energy Fuels* **1998**, *12*, 1191.
[18] S. Talukdar, M. M. Hossain, R. V. Ranganathan, M. Uddi, in *IEEE Int. Conf. on Plasma Science*, IEEE, Piscataway, NJ **2021**.
[19] R. Schlögl, *Angew. Chem. Int. Ed.* **2003**, *42*, 2004.
[20] J. W. Erisman, M. A. Sutton, J. Galloway, Z. Klimont, W. Winiwarter, *Nat. Geosci.* **2008**, *1*, 636.
[21] N. D. Spencer, R. C. Schoonmaker, G. A. Somorjai, *J. Catal.* **1982**, *74*, 129.
[22] R. Vakili, R. Gholami, C. E. Stere, S. Chansai, H. Chen, S. M. Holmes, Y. Jiao, C. Hardacre, X. Fan, *Appl. Catal. B* **2020**, *260*, 118195.
[23] J. A. Andersen, J. M. Christensen, M. Østberg, A. Bogaerts, A. D. Jensen, *Chem. Eng. J.* **2020**, 125519.
[24] J. Martin-del-Campo, M. Uceda, S. Coulombe, J. Kopyscinski, *J. CO2 Util.* **2021**, *46*, 101474.
[25] D. Mei, M. Sun, S. Liu, P. Zhang, Z. Fang, X. Tu, *J. CO2 Util.* **2023**, *67*, 102307.
[26] M. R. Ahasan, M. M. Hossain, Z. Barlow, X. Ding, R. Wang, *ACS Appl. Mater. Interfaces* **2023**, *15*, 44984.
[27] M. Ramakers, I. Michielsen, R. Aerts, V. Meynen, A. Bogaerts, *Plasma Process. Polym.* **2015**, *12*, 755.
[28] K. Van Laer, A. Bogaerts, *Energy Technol.* **2015**, *3*, 1038.
[29] J. Wang, K. Zhang, V. Meynen, A. Bogaerts, *Chem. Eng. J.* **2023**, *465*, 142953.
[30] I. Iliuta, F. Larachi, *Ind. Eng. Chem. Res.* **2020**, *59*, 6815.
[31] A. Berthelot, A. Bogaerts, *J. Phys. Chem. C* **2017**, *121*, 8236.
[32] M. Y. Ong, S. Nomanbhay, F. Kusumo, P. L. Show, *J. Clean. Prod.* **2022**, *336*, 130447.
[33] A. Marafee, C. Liu, G. Xu, R. Mallinson, L. Lobban, *Ind. Eng. Chem. Res.* **1997**, *36*, 632.
[34] C. Liu, A. Marafee, B. Hill, G. Xu, R. Mallinson, L. Lobban, *Ind. Eng. Chem. Res.* **1996**, *35*, 3295.
[35] C. Du, J. Mo, H. Li, *Chem. Rev.* **2015**, *115*, 1503.
[36] M. H. Rafiq, J. E. Hustad, *Ind. Eng. Chem. Res.* **2011**, *50*, 5428.
[37] G. Trenchev, St. Kolev, W. Wang, M. Ramakers, A. Bogaerts, *J. Phys. Chem. C* **2017**, *121*, 24470.
[38] K. Pornmai, N. Arthiwet, N. Rueangjitt, H. Sekiguchi, S. Chavadej, *Ind. Eng. Chem. Res.* **2014**, *53*, 11891.
[39] R. Burlica, K.-Y. Shih, B. R. Locke, *Ind. Eng. Chem. Res.* **2010**, *49*, 6342.
[40] A. Bogaerts, A. Berthelot, S. Heijkers, S. Kolev, R. Snoeckx, S. Sun, G. Trenchev, K. Van Laer, W. Wang, *Plasma Sources Sci. Technol.* **2017**, *26*, 63001.
[41] H. Puliyalil, D. Lašič Jurković, V. D. B. C. Dasireddy, B. Likozar, *RSC Adv.* **2018**, *8*, 27481.
[42] J. Van Turnhout, D. Aceto, A. Travert, P. Bazin, F. Thibault-Starzyk, A. Bogaerts, F. Azzolina-Jury, *Catal. Sci. Technol.* **2022**, *12*, 6676.
[43] L. C. S. Kahle, T. Roussière, L. Maier, K. Herrera Delgado, G. Wasserschaff, S. A. Schunk, O. Deutschmann, *Ind. Eng. Chem. Res.* **2013**, *52*, 11920.
[44] S. T. Oyama, P. Hacarlioglu, Y. Gu, D. Lee, *Int. J. Hydrogen Energy* **2012**, *37*, 10444.
[45] K. Nagaoka, M. Okamura, K. Aika, *Catal. Commun.* **2001**, *2*, 255.
[46] Y. R. Luo, in *Comprehensive Handbook of Chemical Bond Energies*, CRC Press **2007**, pp. 1–1656.
[47] L. Yue, J. Li, C. Chen, X. Fu, Y. Gong, X. Xia, J. Hou, C. Xiao, X. Chen, L. Zhao, G. Ran, H. Wang, *Fuel* **2018**, *218*, 335.
[48] A. Abdulrasheed, A. A. Jalil, Y. Gambo, M. Ibrahim, H. U. Hambali, M. Y. Shahul Hamid, *Renew. Sustain. Energy Rev.* **2019**, *108*, 175.
[49] A. Aziznia, H. R. Bozorgzadeh, N. Seyed-Matin, M. Baghalha, A. Mohamadalizadeh, *J. Nat. Gas Chem.* **2012**, *21*, 466.
[50] E. le Saché, T. R. Reina, *Prog. Energy Combust. Sci.* **2022**, *89*, 100970.
[51] W. C. Chung, M. B. Chang, *Renewable Sustainable Energy Rev.* **2016**, *62*, 13.
[52] M. R. Ahasan, M. M. Hossain, R. Wang, *J. Mater. Chem. A* **2024**, *12*, 29708.
[53] M. M. Hossain, M. R. Ahasan, X. Ding, R. Wang, *Chem. Eng. J.* **2024**, *479*, 147459.
[54] M. R. Ahasan, M. M. Hossain, X. Ding, R. Wang, *J. Mater. Chem. A Mater.* **2023**, *11*, 10993.
[55] P. Mehta, P. Barboun, D. B. Go, J. C. Hicks, W. F. Schneider, *ACS Energy Lett.* **2019**, *4*, 1115.
[56] R. V. Ranganathan, B. Jony, S. M. Fondriest, Z. Liu, R. Wang, M. Uddi, *J. CO2 Util.* **2019**, *32*, 11.
[57] S. W. Benson, *J. Chem. Educ.* **1965**, *42*, 502.
[58] T. Nozaki, K. Okazaki, *Catal. Today* **2013**, *211*, 29.
[59] H. J. Gallon, X. Tu, M. V. Twigg, J. C. Whitehead, *Appl. Catal. B* **2011**, *106*, 616.
[60] J. C. Whitehead, *Pure Appl. Chem.* **2010**, *82*, 1329.
[61] M. Monir Hossain, M. Robayet Ahasan, R. Wang, *Chem. Eng. J.* **2024**, *496*, 154193.
[62] M. Scapinello, E. Delikonstantis, G. D. Stefanidis, *Chem. Eng. Process.* **2017**, *117*, 120.
[63] R. Snoeckx, W. Wang, X. Zhang, M. S. Cha, A. Bogaerts, *Sci. Rep.* **2018**, *8*, 15929.
[64] R. Snoeckx, A. Bogaerts, *Chem Soc Rev.* **2017**, *46*, 5805.
[65] S. Heijkers, M. Aghaei, A. Bogaerts, *J. Phys. Chem. C* **2020**, *124*, 7016.
[66] M. S. Moss, K. Yanallah, R. W. K. Allen, F. Pontiga, *Plasma Sources Sci. Technol.* **2017**, *26*, 035009.
[67] A. H. Khoja, M. Tahir, N. A. S. Amin, *Energy Convers. Manage.* **2019**, *183*, 529.
[68] A. Gómez-Ramírez, V. J. Rico, J. Cotrino, A. R. González-Elipe, R. M. Lambert, *ACS Catal.* **2014**, *4*, 402.
[69] D. Mei, X. Zhu, Y.-L. He, J. D. Yan, X. Tu, *Plasma Sources Sci Technol.* **2014**, *24*, 15011.
[70] G. Petitpas, J. D. Rollier, A. Darmon, J. Gonzalez-Aguilar, R. Metkemeijer, L. Fulcheri, *Int. J. Hydrogen Energy* **2007**, *32*, 2848.
[71] R. Snoeckx, S. Heijkers, K. Van Wesenbeeck, S. Lenaerts, A. Bogaerts, *Energy Environ. Sci.* **2016**, *9*, 999.

[72] K. Krawczyk, M. Młotek, B. Ulejczyk, K. Schmidt-Szałowski, *Fuel* **2014**, *117*, 608.
[73] I. Istadi, N. A. S. Amin, *Chem. Eng. Sci.* **2007**, *62*, 6568.
[74] T. Nozaki, A. Bogaerts, X. Tu, R. Sanden, *Plasma Process. Polym.* **2017**, *14*, 1790061.
[75] S. Kameshima, K. Tamura, R. Mizukami, T. Yamazaki, T. Nozaki, *Plasma Process. Polym.* **2017**, *14*, 1.
[76] L. Brune, A. Ozkan, E. Genty, T. Visart De Bocarmé, F. Reniers, *J. Phys. D Appl. Phys.* **2018**, *51*, 234002.
[77] M. A. Shalabi, S. A. Zaidi, M. A. Al-Saleh, *Chem. Eng. Commun.* **1997**, *157*, 23.
[78] U. Kogelschatz, *Plasma Chem. Plasma Process.* **2003**, *23*, 1.
[79] A. Fridman, *Plasma Chem.* **2008**, *8*, 1.
[80] J. M. Williamson, D. D. Trump, P. Bletzinger, B. N. Ganguly, *J. Phys. D Appl. Phys.* **2006**, *39*, 4400.
[81] N. Jiang, L. Guo, C. Qiu, Y. Zhang, K. Shang, N. Lu, J. Li, Y. Wu, *Chem. Eng. J.* **2018**, *350*, 12.
[82] L. Zhang, D. Yang, W. Wang, S. Wang, H. Yuan, Z. Zhao, C. Sang, L. Jia, *Sci. Rep.* **2016**, *62016*, 1.
[83] S. P. Das, G. Dalei, A. Barik, *IOP Conf. Ser. Mater. Sci. Eng.* **2018**, *410*, 012004.
[84] U. Kogelschatz, B. Eliasson, W. Egli *J. Phys. IV Proc.* **1997**, *07*, C4-47.
[85] D. Amri, Z. Nawawi, M. I. Jambak, *IOP Conf. Ser. Mater. Sci. Eng.* **2019**, *620*, 012091.
[86] T. Shao, C. Zhang, Z. Fang, Y. Yu, D. Zhang, P. Yan, Y. Zhou, E. Schamiloglu, *IEEE Trans. Plasma Sci.* **2013**, *41*, 3069.
[87] G. Duan, Z. Fang, J. Fu, P. Yu, D. Mei, *IEEE Trans. Plasma Sci.* **2021**, *49*, 1173.
[88] D. Mei, G. Duan, J. Fu, S. Liu, R. Zhou, R. Zhou, Z. Fang, P. J. Cullen, K. (Ken) Ostrikov, *J. CO2 Util.* **2021**, *53*, 101703.
[89] A. Ozkan, T. Dufour, G. Arnoult, P. De Keyzer, A. Bogaerts, F. Reniers, *J. CO2 Util.* **2015**, *9*, 74.
[90] A. Bogaerts, E. C. Neyts, *ACS Energy Lett.* **2018**, *3*, 1013.
[91] H. H. Kim, Y. Teramoto, N. Negishi, A. Ogata, *Catal. Today* **2015**, *256*, 13.
[92] D. Mei, X. Tu, *J. CO2 Util.* **2017**, *19*, 68.
[93] C. Xu, X. Tu, *J. Energy Chem.* **2013**, *22*, 420.
[94] A. Ozkan, T. Dufour, T. Silva, N. Britun, R. Snyders, A. Bogaerts, F. Reniers, *Plasma Sources Sci. Technol.* **2016**, *25*, 025013.
[95] S. Y. Liu, D. H. Mei, Z. Shen, X. Tu, *J. Phys. Chem. C* **2014**, *118*, 10686.
[96] R. Snoeckx, Y. X. Zeng, X. Tu, A. Bogaerts, *RSC Adv.* **2015**, *5*, 29799.
[97] A. J. Zhang, A. M. Zhu, J. Guo, Y. Xu, C. Shi, *Chem. Eng. J.* **2010**, *156*, 601.
[98] D. Mei, Y.-L. He, S. Liu, J. Yan, X. Tu, *Plasma Process. Polym.* **2016**, *13*, 544.
[99] X. Wang, Y. Gao, S. Zhang, H. Sun, J. Li, T. Shao, *Appl. Energy* **2019**, *243*, 132.
[100] Y. Zheng, Y. Hao, Z. Cui, *Plasma Chem. Plasma Process.* **2023**, *43*, 1941.
[101] Y. Uytdenhouwen, J. Hereijgers, T. Breugelmans, P. Cool, A. Bogaerts, *Chem. Eng. J.* **2021**, *405*, 126618.
[102] I. Michielsen, Y. Uytdenhouwen, J. Pype, B. Michielsen, J. Mertens, F. Reniers, V. Meynen, A. Bogaerts, *Chem. Eng. J.* **2017**, *326*, 477.
[103] R. Li, Q. Tang, S. Yin, T. Sato, *Fuel Process. Technol.* **2006**, *87*, 617.
[104] I. Michielsen, Y. Uytdenhouwen, A. Bogaerts, V. Meynen, *Catalysts* **2019**, *9*, 51.
[105] K. G. Kostov, R. Y. Honda, L. M. S. Alves, M. E. Kayama, *Braz. J. Phys.* **2009**, *39*, 322.
[106] A. Ozkan, T. Dufour, A. Bogaerts, F. Reniers, *Plasma Sources Sci. Technol.* **2016**, *25*, 045016.
[107] K. Van Laer, A. Bogaerts, *Plasma Process. Polym.* **2017**, *14*, 1600129.
[108] Y. Uytdenhouwen, K. M. Bal, I. Michielsen, E. C. Neyts, V. Meynen, P. Cool, A. Bogaerts, *Chem. Eng. J.* **2019**, *372*, 1253.
[109] M. Okumoto, A. Mizuno, *Catal. Today* **2001**, *71*, 211.
[110] M. Okumoto, H. H. Kim, K. Takashima, S. Katsura, A. Mizuno, *IEEE Trans. Ind. Appl.* **2001**, *37*, 1618.
[111] E. Delikonstantis, M. Scapinello, O. Van Geenhoven, G. D. Stefanidis, *Chem. Eng. J.* **2020**, *380*, 122477.
[112] Y. Uytdenhouwen, S. Van Alphen, I. Michielsen, V. Meynen, P. Cool, A. Bogaerts, *Chem. Eng. J.* **2018**, *348*, 557.
[113] S. L. Brock, T. Shimojo, M. Marquez, C. Marun, S. L. Suib, H. Matsumoto, Y. Hayashi, *J. Catal.* **1999**, *184*, 123.
[114] H. K. Song, H. Lee, J. W. Choi, B. K. Na, *Plasma Chem. Plasma Process.* **2004**, *24*, 57.
[115] D. Ray, R. Saha, C. Subrahmanyam, *Catalysts* **2017**, *7*, 1–11.
[116] D. B. Nguyen, W. G. Lee, *J. Ind. Eng. Chem.* **2015**, *32*, 187.
[117] S. L. Brock, M. Marquez, S. L. Suib, Y. Hayashi, H. Matsumoto, *J. Catal.* **1998**, *180*, 225.
[118] D. Yap, J. M. Tatibouët, C. Batiot-Dupeyrat, *J. CO2 Util.* **2015**, *12*, 54.
[119] H. Sadat, N. Dubus, L. Pinard, J. M. Tatibouet, J. Barrault, *Appl. Therm. Eng.* **2009**, *29*, 1259.
[120] T. Kappes, W. Schiene, T. Hammer, *Hakone-8* **2002**, *21*, 21.
[121] X. Zhang, M. S. Cha, *J. Phys. D Appl. Phys.* **2013**, *46*, 415205.
[122] D. B. Nguyen, Q. H. Trinh, M. M. Hossain, W. G. Lee, Y. S. Mok, *Int. J .Hydrogen Energy* **2020**, *45*, 18519.
[123] G. Neumann, U. Bänziger, M. Kammeyer, M. Lange, *Rev. Sci. Instrum.* **1993**, *64*, 19.
[124] A. Álvarez, M. Borges, J. J. Corral-Pérez, J. G. Olcina, L. Hu, D. Cornu, R. Huang, D. Stoian, A. Urakawa, *ChemPhysChem* **2017**, *18*, 3135.
[125] X. Xiaoding, J. A. Moulijn, *Energy Fuels* **1996**, *10*, 305.
[126] A. Holmen, *Catal. Today* **2009**, *142*, 2.
[127] F. Farshchi Tabrizi, S. A. H. S. Mousavi, H. Atashi, *Energy Convers. Manage.* **2015**, *103*, 1065.
[128] N. Bouchoul, E. Fourré, J. M. Tatibouët, C. Batiot-Dupeyrat, *Plasma Chem. Plasma Process.* **2019**, *39*, 713.
[129] J. F. Gelves, L. Dorkis, M. Marquez, E. Fourré, C. Batiot-Dupeyrat, *J. Phys. Conf. Ser.* **2019**, *1386*, 012045.
[130] H. Wang, J. Han, Z. Bo, L. Qin, Y. Wang, F. Yu, *Mol. Catal.* **2019**, *475*, 110486.
[131] D. Li, V. Rohani, F. Fabry, A. Parakkulam Ramaswamy, M. Sennour, L. Fulcheri, *Appl. Catal. B* **2020**, *261*, 2.
[132] D. Mei, X. Zhu, C. Wu, B. Ashford, P. T. Williams, X. Tu, *Appl. Catal. B* **2016**, *182*, 525.
[133] D. Mei, X. Zhu, Y. L. He, J. D. Yan, X. Tu, *Plasma Sources Sci Technol.* **2014**, *24*, 015011.
[134] E. Jwa, S. B. Lee, H. W. Lee, Y. S. Mok, *Fuel Process. Technol.* **2013**, *108*, 89.
[135] R. Benrabbah, C. Cavaniol, H. Liu, S. Ognier, S. Cavadias, M. E. Gálvez, P. Da Costa, *Catal. Commun.* **2017**, *89*, 73.
[136] M. Nizio, A. Albarazi, S. Cavadias, J. Amouroux, M. E. Galvez, P. Da Costa, *Int. J. Hydrogen Energy* **2016**, *41*, 11584.
[137] Y. Sun, J. Li, P. Chen, B. Wang, J. Wu, M. Fu, L. Chen, D. Ye, *Appl. Catal. A Gen.* **2020**, *591*, 117407.

Md Robayet Ahasan is a module development engineer, Intel Corporation. His current work focuses on reactive ion etching (RIE) or plasma etching of silicon, metal, and dielectric materials, defining the key structures of the transistors, and determining many aspects of device performance. He received his Ph.D. from the University of Alabama in 2024. Prior to joining Intel, Dr. Ahasan was a graduate research assistant in the Department of Metallurgical and Materials Engineering at the University of Alabama under the supervision of Dr. Ruigang Wang. He studied plasma-assisted catalysis to effectively and efficiently convert various greenhouse gases into value-added fuels and chemicals.

Md Monir Hossain is a Ph.D. candidate in the Department of Chemical Engineering and Materials Science at Michigan State University, focusing on DBD plasma catalysis to enhance syngas production. His research explores the effects of nanoshaped catalysts on dry reforming of methane reactions, aiming to optimize catalyst–plasma interactions for improved efficiency. Monir has authored multiple peer-reviewed publications on plasma-assisted catalysis, examining factors like catalyst morphology, coke formation pathways, and reaction mechanisms. With extensive experience in materials characterization (e.g., SEM, TEM, XPS) and gas analysis (e.g., QMS, GC, spectroscopy), he brings a solid technical foundation to his work.

Ruigang Wang is a professor in the Department of Chemical Engineering and Materials Science at Michigan State University. He received his Ph.D. in materials science and engineering from Arizona State University in 2007 studying in situ environmental transmission electron microscopy and completed postdoctoral studies of fuel cells and Li-ion batteries at Materials Sciences Division of Lawrence Berkeley National Lab from 2007 to 2010. His research interests include energy storage materials (metal–sulfur batteries, aluminum-ion battery, lithium-ion battery, and all solid-state batteries), and emission control catalysts (i.e., for plasma-assisted CO_2 hydrogenation, dry reforming of methane, and automotive catalytic converter), and chemical metallurgy.